THE JOURNAL OF BIOLOGICAL CHEMISTRY VOL. 282, NO. 1, pp. 637–646, January 5, 2007

Spatial Expression Patterns and Biochemical Properties Distinguish a Second *myo*-Inositol Monophosphatase IMPA2 from IMPA1*[S]

Received for publication, May 10, 2006, and in revised form, October 2, 2006 Published, JBC Papers in Press, October 26, 2006, DOI 10.1074/jbc.M604474200

Tetsuo Ohnishi[‡1], Hisako Ohba[‡], Kyung-Chang Seo[§], Jungkyun Im[§], Yumi Sato[¶], Yoshimi Iwayama[‡], Teiichi Furuichi[¶], Sung-Kee Chung[§], and Takeo Yoshikawa[‡‖]

From the [‡]Laboratory for Molecular Psychiatry, RIKEN Brain Science Institute, Wako, Saitama 351-0198, Japan, [§]Department of Chemistry, Division of Molecular and Life Sciences, Pohang University of Science & Technology, Pohang 790-784, South Korea, [¶]Laboratory for Molecular Neurogenesis, RIKEN Brain Science Institute, Wako, Saitama 351-0198, Japan, and [‖]Core Research for Evolutional Science & Technology (CREST), Japan Science and Technology Agency, Saitama 332-0012, Japan

Lithium is used in the clinical treatment of bipolar disorder, a disease where patients suffer mood swings between mania and depression. Although the mode of action of lithium remains elusive, a putative primary target is thought to be inositol monophosphatase (IMPase) activity. Two IMPase genes have been identified in mammals, the well characterized *myo*-inositol monophosphatase 1 (*IMPA1*) and *myo*-inositol monophosphatase 2 (*IMPA2*). Several lines of genetic evidence have implicated *IMPA2* in the pathogenesis of not only bipolar disorder but also schizophrenia and febrile seizures. However, little is known about the protein, although it is predicted to have lithium-inhibitable IMPase activity based on its homology to IMPA1. Here we present the first biochemical study comparing the enzyme activity of IMPA2 to that of IMPA1. We demonstrate that *in vivo*, IMPA2 forms homodimers but no heterodimers with IMPA1. Recombinant IMPA2 exhibits IMPase activity, although maximal activity requires higher concentrations of magnesium and a higher pH. IMPA2 shows significantly lower activity toward *myo*-inositol monophosphate than IMPA1. We therefore screened for additional substrates that could be more efficiently dephosphorylated by IMPA2, but failed to find any. Importantly, when using *myo*-inositol monophosphate as a substrate, the IMPase activity of IMPA2 was inhibited at high lithium and restricted magnesium concentrations. This kinetics distinguishes it from IMPA1. We also observed a characteristic pattern of differential expression between *IMPA1* and *IMPA2* in a selection of tissues including the brain, small intestine, and kidney. These data suggest that IMPA2 has a separate function *in vivo* from that of IMPA1.

Inositol monophosphatase (IMPase[2]; EC 3.1.3.25) is an enzyme that dephosphorylates *myo*-inositol monophosphate to generate free *myo*-inositol. This enzymatic pathway is important in cellular functions because *myo*-inositol is a precursor of the membrane phospholipid, phosphatidylinositol (PI). PI and its phosphorylated derivatives (phosphatidylinositol phosphate; PIP) play crucial roles in intracellular signal transduction via the production of second messengers, *myo*-inositol 1,4,5-trisphosphate, and diacylglycerol. Inositol 1,4,5-trisphosphate triggers release of Ca^{2+} from intracellular stores and undergoes a multi-step dephosphorylation by multiple enzymes including IMPase to generate free *myo*-inositol. Cells can generate *myo*-inositol by another biochemical pathway in which glucose 6-phosphate is isomerized by *myo*-inositol 1-phosphate synthase to produce *myo*-inositol 1-phosphate (1) and then dephosphorylated by IMPase leading to free *myo*-inositol. The dephosphorylation of *myo*-inositol monophosphate by IMPase is a critical and rate-limiting step for the regeneration of PI.

From a clinical point of view, IMPase has attracted much interest (1–4). Bipolar disorder (also known as manic depressive illness) is characterized by chronically recurring episodes of fluctuating moods between mania and depression. Lithium has been used for half a century as a first-line drug in this disorder. Importantly, lithium inhibits IMPase under therapeutic concentrations (~1 mM). Besides IMPase, several other enzymes (inositol polyphosphate phosphatase, bisphosphate nucleotidase, fructose 1,6-bisphophatase, phosphoglucomutase, and glycogen synthase kinase-3β) have been proposed as possible targets of lithium (4–6). However, it is unclear as to which molecule is central to the efficacy of lithium.

Berridge *et al.* (7, 8) proposed the "inositol depletion hypothesis" in the therapy of bipolar disorder. It suggests that the beneficial effect of lithium in the treatment of this disease is at least partly mediated by the inhibition of IMPase. Lithium is thought to suppress *myo*-inositol production by inhibiting IMPase and/or inositol polyphosphatase, in turn, attenuating the production of the PI-related

* This work was supported in part by grant-in-aid from the Ministry of Education, Culture, Sports, Science and Technology (to T. O. and T. Y.), a grant from Mitsubishi Pharma Research Foundation (to T. Y.), and an Astra Zeneca research grant (to T. O.). The synthetic work at Postech was supported by a grant from Korea Institute of Science and Technology Evaluation and Planning/Korea Science and Engineering Foundation (Biotechnology program-Glycobiology 2004-02087). The costs of publication of this article were defrayed in part by the payment of page charges. This article must therefore be hereby marked "*advertisement*" in accordance with 18 U.S.C. Section 1734 solely to indicate this fact.

[S] The on-line version of this article (available at http://www.jbc.org) contains supplemental Fig. 1.

[1] To whom correspondence should be addressed: Laboratory for Molecular Psychiatry, RIKEN Brain Science Inst., 2-1 Hirosawa, Wako, Saitama 351-0198, Japan. Tel.: 81-48-467-5946; Fax: 81-48-467-7462; E-mail: tohnishi@brain.riken.jp.

[2] The abbreviations used are: IMPase, inositol monophosphatase; PIP, phosphatidylinositol phosphate; HA, hemagglutinin; siRNA, small interfering RNA; MES, 2-(*N*-morpholino)ethanesulfonic acid; PIPES, piperazine-*N*,*N*′-bis(2-ethanesulfonic acid).

Supplemental Material can be found at: http://www.jbc.org/cgi/content/full/M604474200/DC1

second messengers, *myo*-inositol 1,4,5-trisphosphate, and diacylglycerol. Interestingly, Williams *et al.* (9) observed that lithium and two other mood stabilizers, carbamazepine and valproic acid, blocked the collapse of sensory neuron growth cones and expanded the growth cone area. These effects were reversed by supplementation of inositol in the medium. These data support the idea that inositol depletion may underlie the action of mood stabilizers.

To date *IMPA1* is the only gene known to encode IMPase activity (10, 11). The *IMPA1* gene product has a close homolog, *IMPA2*. *IMPA2* has attracted much attention in the genetic studies of neuropsychiatric diseases (12–14) because of a possible biochemical and cellular signaling role analogous to that of IMPA1 and its chromosomal position on 18p11.2 (15), a susceptibility locus not only for bipolar disorder but also schizophrenia and lately febrile seizures. Genetic associations between *IMPA2* polymorphisms and schizophrenia (12) and febrile seizures (13) have been demonstrated. Recently, Sjøholt *et al.* (14) and unpublished data from our group[3] have shown genetic associations between this gene and bipolar disorder in Palestinian Arabs (14) and Japanese samples, respectively. We have detected up-regulation of *IMPA2* mRNA in postmortem brains from bipolar patients that harbor risk promoter single nucleotide polymorphisms.[3]

Despite intensive analyses, there is no genetic evidence linking *IMPA1* to mental disorders (14). The protein is, however, well characterized biochemically. First, IMPA1 exhibits magnesium-dependent IMPase activity, which is inhibited by therapeutic doses of lithium. Second, the protein forms homodimers and is abundantly expressed in the brain. X-ray crystallographic studies have revealed the three-dimensional structure of the IMPA1 homodimer (16). In contrast, no information was available on the biochemical or structural properties of IMPA2. It was not known whether the gene was translated *in vivo* or the gene product displayed IMPase activity as predicted by its structural homology with IMPA1. This study aimed to characterize the function of *IMPA2* by examining its biochemical and expressional profiles as a first step to investigating the cellular role of this gene in the pathogenesis of multiple neuropsychiatric disorders.

EXPERIMENTAL PROCEDURES

Cells and Antibodies—NB-1 and IMR-32 cell lines were purchased from the Japanese Collection of Research Bioresources (Tokyo, Japan). The HeLa Tet-Off cell line was from Clontech (Mountain View, CA). MIA-PaCa2 and Panc-1 cells were from ATCC (Manassas, VA). Anti-IMPA2 rabbit antisera were raised against two IMPA2 peptides (IMPA2-N, ALAGGIIRKALTEEKC and IMPA2-C, CALQTINYGRDDEK) that were coupled to keyhole lympet hemocyanin. Anti-IMPA1 serum was raised against the IMPA1 peptide, EAIKNEMNVMLKSSVDLC.

Northern Blot Analysis—Total RNA was extracted from cell lines using Isogen reagent (Wako Pure Chemicals). Northern blot analysis was performed following standard procedures, using ^{32}P-labeled fragments corresponding to the full open reading frame of human *IMPA1* or *IMPA2* as a probe. *IMPA1* and *IMPA2* fragments were amplified by PCR using the primer sets (5′-GGATTATGCAGTAACTCTAGCAAG-3′ and 5′-GGATTATGCAGTAACTCTAGCAAG-3′ for *IMPA1*; and 5′-ATGAAGCCGAGCGGCGAGGA-3′ and 5′-CATCGCCATCTCCCGGGTGCTG-3′ for *IMPA2*). The fragments were radiolabeled using the Rediprime II DNA labeling system (GE Healthcare) and [α-^{32}P]dCTP (GE Healthcare).

In situ Hybridization—Mouse cDNAs for *IMPA1* and *IMPA2* were amplified by PCR using Marathon-ready mouse brain cDNA (Clontech) and primer sets (5′-GTTGAGCATCGATCGCGGTGCGCT-3′ and 5′-TCCATCTAATTTTGAATATGTCATCTGT-3′ for *IMPA1*; and 5′-AAGGCGAGGGCACTGTGCGGAGCCTCCG-3′ and 5′-CAAGATCTGGGTTTGGCTCTGATGA-3′ for *IMPA2*), then cloned into pBS-KS(+). Digoxigenin-labeled riboprobes were generated using a digoxigenin RNA labeling kit (Roche Applied Science) with T7 or T3 polymerase. *In situ* hybridization of mouse tissues at postnatal days 7 and 21 was performed as described (17). Tissues from adult mice were also examined using the same probes.

Mammalian Expression Vectors—Human *IMPA1* and *IMPA2* cDNAs were cloned into mammalian expression vectors SR-HA and SR-V5 (18, 19) to generate SR-HA-IMPA1, SR-HA-IMPA2, SR-V5-IMPA1, and SR-V5-IMPA2. Site-directed mutagenesis was performed using a standard procedure to generate expression vectors for HA-IMPA1 D93N and HA-IMPA2 D104N.

Immunofluorescent Staining and Cell Fractionation Study—Immunofluorescent staining of overexpressed IMPA proteins was performed as follows: HeLa Tet-Off cells, grown on a glass coverslips, were transfected using Lipofectamine 2000 reagent (Invitrogen) with the stated plasmid. Forty-eight hours after transfection with either SR-HA-IMPA1 or SR-HA-IMPA2 constructs, cells were fixed with cold methanol:acetone (1:1) for 15 min. After blocking in phosphate-buffered saline with 1% bovine serum albumin and 0.05% phosphate buffered saline Tween 20 (PBS-T) for 1 h, the slips were incubated with rat anti-HA monoclonal antibody for 1 h at room temperature. Incubation with secondary antibody (Alexa588-labeled anti-rat IgG, Invitrogen) and 4′,6-diamidino-2-phenylindole, dihydrochloride staining for 1 h at room temperature were followed by washes in PBS-T. Fractionation of HeLa Tet-Off cells was performed using the FractionPREP Cell Fractionation system (Biovision, Mountain View, CA) following the manufacturer's instructions. We used the following antibodies as localization markers: anti-Hsp70 (Sigma) and anti-Akt1 (Cell Signaling, Danvers, MA) as cytoplasmic markers; anti-pan-cadherin (Sigma) and anti-cytochrome P450 reductase (Santa Cruz Biotechnology, Santa Cruz, CA) as membrane markers; anti-histone H1 (Upstate, Lake Placid, NY) as a nuclear marker; and anti-vimentin (Sigma) as a cytoskeletal marker.

Knockdown of Inositol Monophosphatase Proteins by Small Interfering RNA—Transfection of siRNA duplexes (Stealth siRNA from Invitrogen) into HeLa Tet-Off cells was performed using HiPerFect reagent (Qiagen, Valencia, CA), according to

[3] T. Ohnishi, K. Yamada, H. Ohba, Y. Iwayama, T. Toyota, T. Inada, H. Kunugi, M. Tatsumi, N. Ozaki, N. Iwata, K. Sakamoto, Y. Iijima, Y. Iwata, K. Tsuchiya, G. Sugihara, S. Nanko, N. Osumi, S. D. Detera-Wadleigh, T. Kato, and T. Yoshikawa, manuscript in preparation.

the manufacturer's instructions. Briefly, 12 h before transfection, cells were seeded onto a 24-well plate at a density of 4×10^4/well in normal growth medium and then placed at 37 °C in a 5% CO_2 atmosphere. Just before transfection, wells were emptied, and 500 μl of fresh medium was added. The siRNAs were diluted in 100 μl of normal growth medium without serum and mixed with 1 μl of HiPerFect reagent. After 15-min incubation at room temperature, the complexes were added dropwise to each well. The final siRNA concentration was kept at 5 nM. Forty-eight hours after transfection, cells were harvested in 100 μl of 1.5× SDS sample buffer and boiled at 100 °C for 4 min. After sonication to reduce viscosity, the samples were stored at −20 °C until use. To test the effects of siRNA treatment on cell growth, cells were detached from 6-well dishes by trypsinization at days 1, 2, and 3 post-transfection and counted using a Burker-Turk hemocytometer.

Gel Filtration and Immunoprecipitation—HEK293T cells grown on five 10-cm dishes were transfected with SR-V5-IMPA2 using Lipofectamine 2000 reagent. Two days after transfection, cells were homogenized in lysis buffer containing 25 mM Tris-HCl (pH 7.5), 150 mM NaCl, 1 mM EDTA, 0.2% Tween 20, and protease inhibitors (10 μg/ml leupeptin and 0.2 mM phenylmethylsulfonyl fluoride), using a glass-Teflon homogenizer. Crude cell extract was centrifuged at 100,000 × *g* and 4 °C for 30 min, then frozen at −80 °C until analysis. A portion of the supernatant was analyzed by gel filtration column chromatography (Superdex 200 HR 10/30, GE Healthcare) equipped with the AKTA system (GE Healthcare) at a flow rate of 0.25 ml/min using lysis buffer. Each fraction was Western blotted using the anti-V5 antibody (Promega, Madison, WI). Molecular weight markers (GE Healthcare) were separately run.

Recombinant Proteins—Preparation of HA-tagged recombinant protein from cDNA-transfected HEK293T cells was performed as described (18, 19). After the addition of 25% glycerol, purified protein was frozen at − 80 °C until use. Each preparation was checked for quality by SDS-PAGE followed by Western blot analysis and silver staining.

Phosphatase Assays—Standard assays were performed at 37 °C in the presence of 50 mM Tris-HCl, (pH 8.0) 0.1 mM EGTA, 1 mM substrate, and 70 ng of purified protein in a 20 μl of assay volume. At specified time points, 40 μl of distilled water and 100 μl of Biomol Green reagent (BIOMOL Research Lab., Plymouth Meeting, PA) were added to 10 μl of the reaction. The amount of free phosphate was calculated by calorimetric determination at 620 nm in a micro-titer plate format.

Substrates—The regioisomers of *scyllo*-inositol phosphates and *myo*-inositol phosphates were synthesized according to published procedures (20–22). Commercially available compounds including inositol polyphosphates and other sugar phosphates were purchased from Bachem (Torrance, CA), Wako Pure Chemicals, Alexis (Lausen, Switzerland), Nacalai Tesque (Kyoto, Japan), Calbiochem, AG Scientific (San Diego, CA), and/or Sigma.

RESULTS

Expression of IMPA2—First, we compared the precise spatial expression patterns of *IMPA1* and *IMPA2* in the mouse brain by *in situ* hybridization (Fig. 1). *IMPA1* mRNA showed moderate to high levels of expressions in wide areas of the brain. In contrast, *IMPA2* generally displayed lower levels of expression except for the mid-hind brain regions and cells of the visual cortex, where high expression was maintained. In P7 mouse brains, *IMPA1* mRNA was expressed at high levels in the hippocampus and cerebellar granule cells and Purkinje cells and at moderate levels in the olfactory bulb, cerebral cortex, caudate-putamen, thalamus, superior and inferior colliculus, pontine nuclei, pituitary gland, and medulla oblongata (Fig. 1*A*). In the same stage animals, *IMPA2* mRNA was expressed at relatively high levels in cerebellar Purkinje cells, pons, pituitary gland, and medulla oblongata and at moderate levels in the olfactory bulb, cerebral cortex, hippocampus, and inferior colliculus (Fig. 1*C*). In P21 mouse brains, *IMPA1* mRNA was localized at high levels in the olfactory bulb, hippocampus, and cerebellum and at moderate levels in the caudate-putamen, thalamus, hypothalamus, superior and inferior colliculus, mesencephalic tegmentum, pontine nuclei, and medulla oblongata (Fig. 1*B*), whereas *IMPA2* expression was detected at high levels in the visual cortex (layers II, III, and V), mesencephalic tegmentum, pons, and medulla oblongata (Fig. 1*D*). In P21 olfactory bulb, both *IMPA1* and *IMPA2* mRNAs were expressed in cells of the glomerular layer, mitral cell layer, and granular layer (Fig. 1, *E* and *F*). In P21 hippocampus, *IMPA1* was widely expressed in the CA1–3 regions and dentate gyrus (Fig. 1*G*) at high levels, whereas *IMPA2* was expressed at low levels in cells of similar hippocampal regions (Fig. 1*H*) and the hilus (Fig. 1*O*). In P21 cerebral cortex (motor area), the predominant expression of *IMPA1* was observed in cells of the layers II-III and V (Fig. 1*I*), whereas *IMPA2* mRNA was seen in layer V pyramidal cells (Fig. 1*J*). In P21 cerebellum, *IMPA1* mRNA was detected predominantly in Purkinje cells and moderately in granule cells and deep cerebellar nuclei (Fig. 1, *K* and *M*), whereas *IMPA2* mRNA was localized predominantly in the deep cerebellar nuclei and at low levels in Purkinje cells and cell type(s) of the granular layer (Fig. 1, *L*, *N*, and *P*). These results demonstrated that transcription of *IMPA1* and *IMPA2* was differentially regulated in region and cell-type specific manner within the central nervous system.

Next, we compared the expression of *IMPA2* mRNA with that of *IMPA1* in several human cell lines (Fig. 2*A*). Consistent with our previous data showing the high expression of *IMPA2* mRNA in the pancreas (15), *IMPA2* was expressed as a doublet in two cell lines derived from pancreatic cancers (MIA-PaCa1 and Panc1) in addition to HeLa Tet-Off cells. No expression was detected in two neuroblastoma cell lines (IMR-32 and NB-1). This cell line-specific expression is interesting because the promoter sequence of *IMPA2* has a high G/C content and no canonical TATA box, indicative of a housekeeping gene (23). *IMPA1* mRNA was detected as a single band in all cell lines examined.

To determine whether *IMPA2* transcripts were translated into protein, we attempted to detect IMPA2 protein using HeLa Tet-Off cells expressing *IMPA2* mRNA. We raised two IMPA2 polyclonal antibodies against N- and C-terminal regions (IMPA2-N and IMPA2-C, Fig. 2*B*). Both antibodies consis-

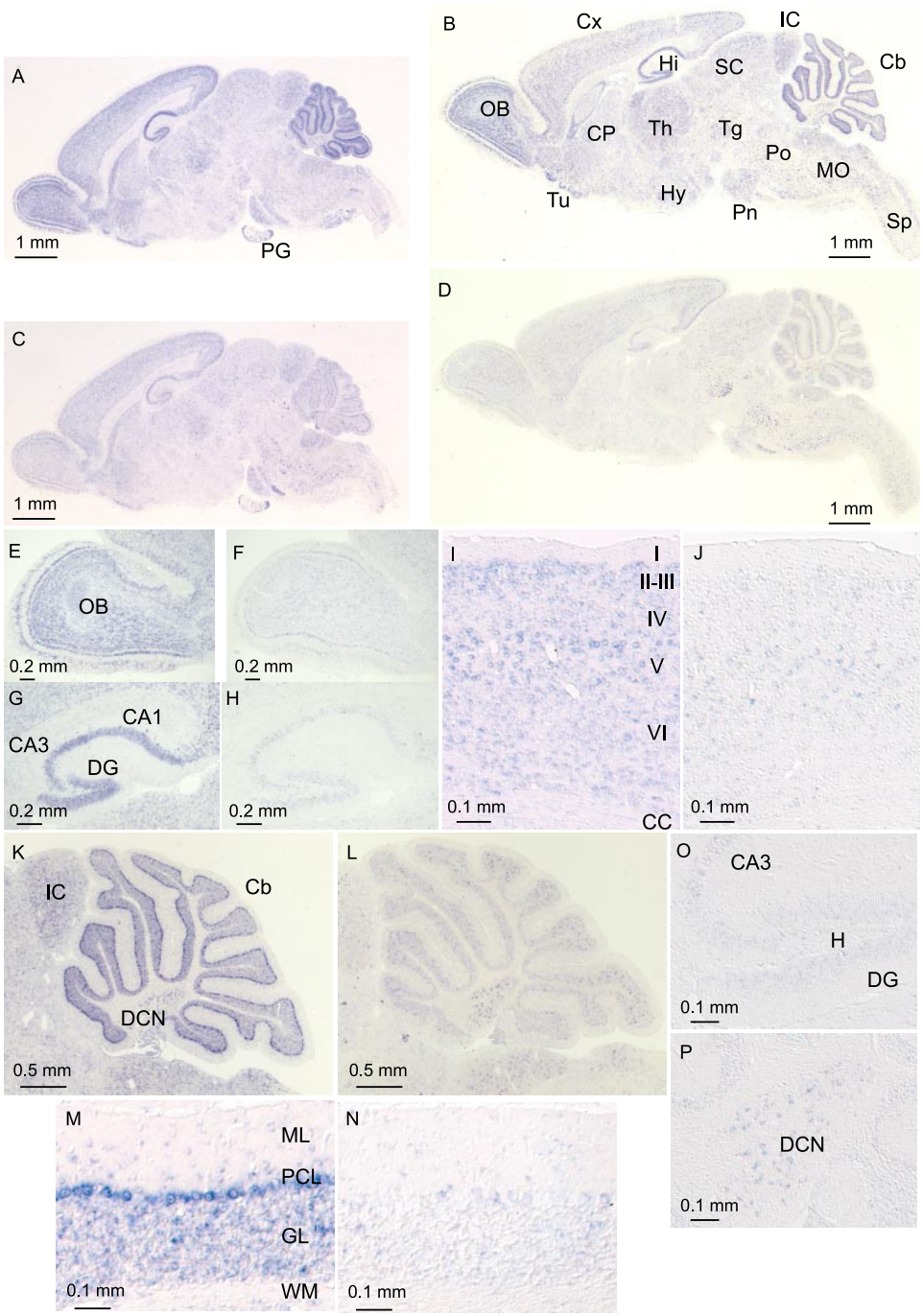

FIGURE 1. **Cellular localizations of *IMPA1* and *IMPA2* mRNAs in sagittal sections of mouse brains at P7 and P21 by *in situ* hybridization.** *A* and *B*, *IMPA1* mRNA in P7 and P21 brains, respectively. *C* and *D*, *IMPA2* mRNA in P7 and P21 brains, respectively. *E* and *F*, *IMPA1* and *IMPA2* mRNAs in P21 olfactory bulbs, respectively. *G* and *H*, *IMPA1* and *IMPA2* mRNAs in P21 hippocampus, respectively. *I* and *J*, *IMPA1* and *IMPA2* mRNAs in P21 cerebral cortex (motor area), respectively. *K* and *L*, *IMPA1* and *IMPA2* mRNAs in P21 cerebellum, respectively. *M* and *N*, *IMPA1* and *IMPA2* mRNAs in P21 cerebellar cortex, respectively. *O* and *P*, *IMPA2* mRNA in the hippocampal hilar region and deep cerebellar nuclei of P21 mice, respectively. *CA1*, hippocampal CA1 region; *CA3*, hippocampal CA3 region; *Cb*, cerebellum; *CC*, corpus callosum; *CP*, caudate-putamen; *Cx*, cerebral cortex; *DCN*, deep cerebellar nuclei; *DG*, dentate gyrus; *GL*, granular layer; *H*, hilus; *Hi*, hippocampus; *Hy*, hypothalamus; *IC*, inferior colliculus; *ML*, molecular layer; *MO*, medulla oblongata; *OB*, olfactory bulb; *PCL*, Purkinje cell layer; *PG*, pituitary gland; *Pn*, pontine nuclei; *Po*, Pons; *SC*, superior colliculus; *Sp*, spinal cord; *Tg*, mesencephalic tegmentum; *Th*, thalamus; *Tu*, olfactory tubercle; *WM*, white matter; *I*, *II-III*, *IV*, *V*, and *VI*, cortical layers I, II-III, IV, V and VI.

tently detected a doublet (31 and 32.5 kDa) in HeLa Tet-Off cell lysates (Fig. 2*C*). Moreover, the intensity of the doublet was significantly reduced in cells treated with siRNAs targeting three different sites on the *IMPA2* transcript (Fig. 2*C*, *lanes 5*, *6*, and *7*), indicating that both proteins in the doublet were immunologically IMPA2. This was the first demonstration that the *IMPA2* gene was translated into protein *in vivo*.

Using our antibodies, we examined the expression of IMPA1 and IMPA2 proteins in mouse tissues. Both proteins were expressed in a range of tissues at different intensities (Fig. 2*D*). This is the first identification of the IMPA2 protein in four regions of the brain, small intestine, heart, kidney, spleen, and other tissues. The major IMPase protein in heart may be IMPA2 because we were unable to detect IMPA1 expression in that organ. The IMPA1 protein was most abundantly expressed in the testis, whereas IMPA2 showed only weak expression. An *in situ* hybridization study using adult mice also showed characteristic expression patterns of two IMPase genes (supplemental Fig. 1). Kidney and small intestine expressed both IMPA1 and IMPA2 proteins with a characteristic difference in their mRNA expression patterns: in the small intestine, *IMPA1* mRNA was strongly expressed in epithelial cells of villi and intestinal glands (Fig. 2*E*, *upper panels*). In contrast, *IMPA2* mRNA was almost exclusively expressed in epithelial cells of intestinal glands (Fig. 2*E*, *lower panels*). In the kidney, strong *IMPA2* signal was observed in the cells surrounding the lumen in the duct-like structures, whereas *IMPA1* expression was ubiquitous. The *IMPA2* positive duct-like structures (Fig. 2*F*, *bottom*, *arrowheads*) are likely to be epithelial cells of the distal convoluted tubules as deduced from their packed nuclear morphology. This anatomical site-specific expression of *IMPA1* and *IMPA2* strongly suggests distinct biological roles in these tissues. We also examined whole brain, spleen, pancreas, and liver for the expression of *IMPA1* and *IMPA2* transcripts from adult mice (supplemental Fig. 1). Consistent with Western blot data, we observed the expression of two transcripts in the brain and spleen (supplemental Fig. 1, *A* and *B*, respectively).

Purification of IMPase from several tissues including brain suggests that it is a predominantly cytosolic protein (24–26).

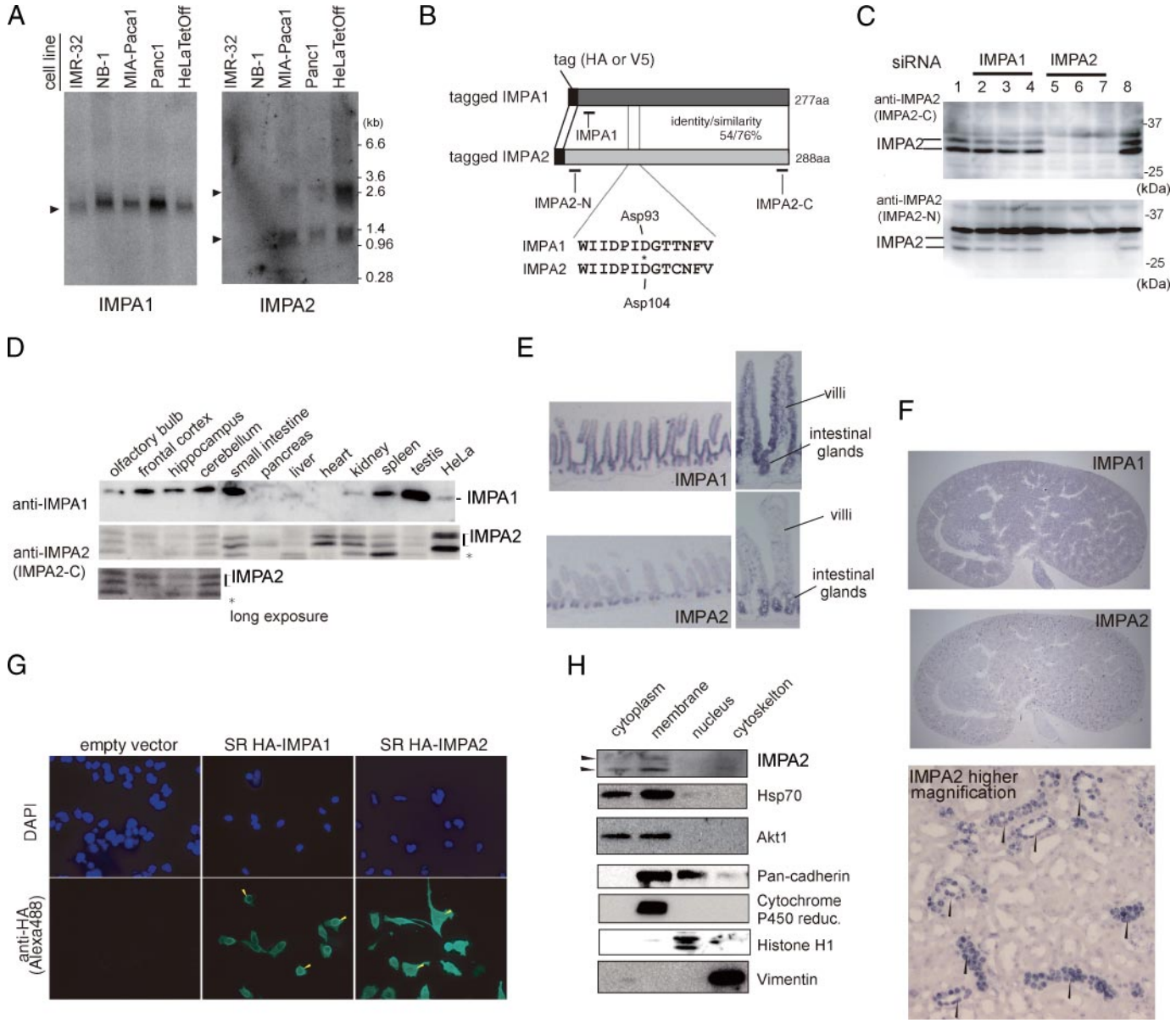

FIGURE 2. **Identification of the *IMPA2* gene product.** *A*, Northern blot showing the expression of *IMPA1* (*left*) and *IMPA2* (*right*) in five cell lines derived from human tumors. *B*, schematic representation of IMPA1 and IMPA2. Recombinant IMPA1 and IMPA2 were expressed as N-terminal HA- or V5-tagged protein in mammalian cells. The amino acid sequence surrounding the Asp-104 of IMPA2, which was mutated to Asn-104 (indicated by an *asterisk*) in HA-IMPA2 D104N, was aligned with the corresponding amino acid sequence of IMPA1. Positions against which the IMPA2 antisera, IMPA2-N and IMPA2-C, and IMPA1 antiserum were targeted, are shown with *bars*. *C*, identification of the IMPA2 protein. HeLa Tet-Off cells were transfected with siRNA targeting *IMPA1* (*lanes 2*, *3*, and *4*), *IMPA2* (*lanes 5*, *6*, and *7*), or lamin A/C (*lane 8*). Control siRNA (*lane 1*) was also used. Lysates from siRNA-treated cells were analyzed by Western blotting with anti-IMPA2 antibodies, IMPA2-C (*top*), and IMPA2-N (*bottom*). Mixtures for three sets of siRNA duplexes targeting three different sites on each mRNA were used for *IMPA1* and *IMPA2*. *D*, tissue distribution of endogenous IMPA1 and IMPA2 proteins. Solubilized proteins (40 μg each) from various mouse tissues were analyzed by Western blotting with anti-IMPA1 (*top*) and anti-IMPA2 (IMPA2-C) (*middle*). The long exposure image of IMPA2-C antibody hybridization is also shown to demonstrate the expression of the IMPA2 protein in the brain (*bottom*). *E*, *in situ* hybridization of small intestine from adult mice. Images at lower (*left*) and higher (*right*) magnifications are shown for *IMPA1* and *IMPA2* transcripts (*upper* and *lower panels*, respectively). *F*, *in situ* hybridization of kidney from adult mice. Images for *IMPA1* (*top*) and *IMPA2* (middle) transcripts are shown. *Arrowheads* indicate *IMPA2*-positive duct-like structures, possible distal convoluted tubules. *G*, cellular localization of transiently expressed HA-IMPA1 and HA-IMPA2. Cells transfected with empty vector (*left*), SR-HA-IMPA1 (*center*), or SR-HA-IMPA2 (*right*) were immunostained with anti-HA antibody (lower, *green*). Perinuclear staining by the HA-antibody is denoted by *arrowheads*, and 4′,6-diamidino-2-phenylindole-stained images (*blue*) of the same view fields are shown in the *top row*. *H*, cellular fractionation of HeLa Tet-Off cells. Each fraction was examined by Western blotting using antibody against the indicated protein.

HA-tagged IMPA2 (Fig. 2*B*) expressed in HeLa Tet-Off cells showed a dispersed pattern in the cytoplasm and nucleus (Fig. 2*G*). This pattern was similar to that of IMPA1. Perinuclear staining (Fig. 2*G*, *arrowheads*) was observed with both HA-IMPA1 and -IMPA2 constructs. These nuclear-associated stainings are possibly artifacts generated by the overexpression system. This speculation is supported by a biochemical fractionation study of HeLa Tet-Off cells (Fig. 2*H*), indicating the absence of IMPA2 protein in the nuclear fraction. The majority of IMPA2 protein was detected in the cytoplasmic and membrane fractions. Because the two cytoplasmic markers used in this study, Hsp70 and Akt1, were detected as contaminants in

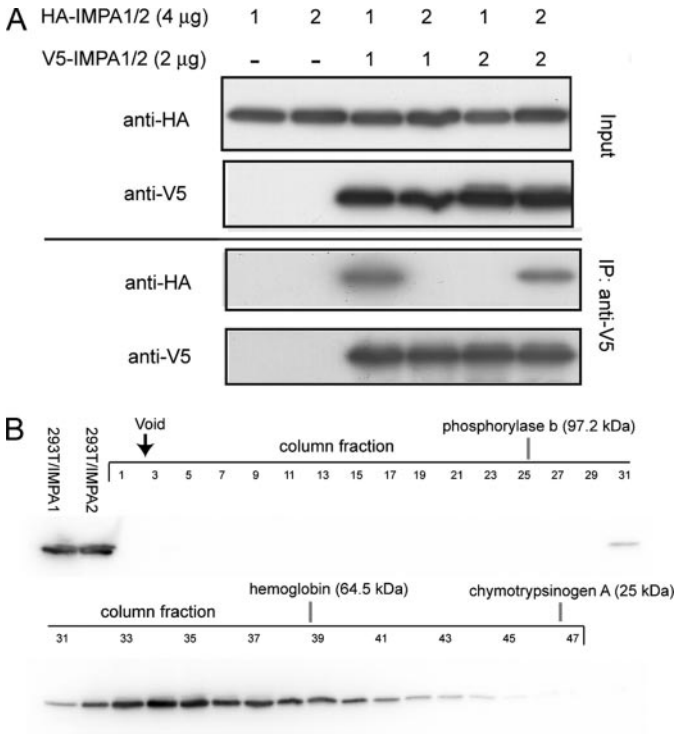

FIGURE 3. **Homodimerization of IMPA2.** *A*, Co-immunoprecipitation assay. HEK293T cells were transfected with either V5-IMPA1, -IMPA2 constructs, or empty vector (−) in combination with a vector expressing HA-IMPA1 or -IMPA2. After a 2 day incubation, cell lysates were immunoprecipitated with the V5 antibody. The immunoprecipitates (*IP*) and cell lysates (*Input*, *top two panels*) were analyzed by Western blotting with anti-HA or -V5 antibody. *B*, gel filtration assay. Lysates from cells transfected with plasmid expressing V5-IMPA2 were run on gel filtration column chromatography. Each fraction and the lysate from cells expressing V5-IMPA1 (*left most lane*) or -IMPA2 (*second lane from left*) were analyzed by Western blotting using the V5 antibody. Fraction numbers (1 through 47) are shown. Elution points for molecular weight markers (*phosphorylase b*, *hemoglobin*, and *chymotrypsinogen A*) are indicated.

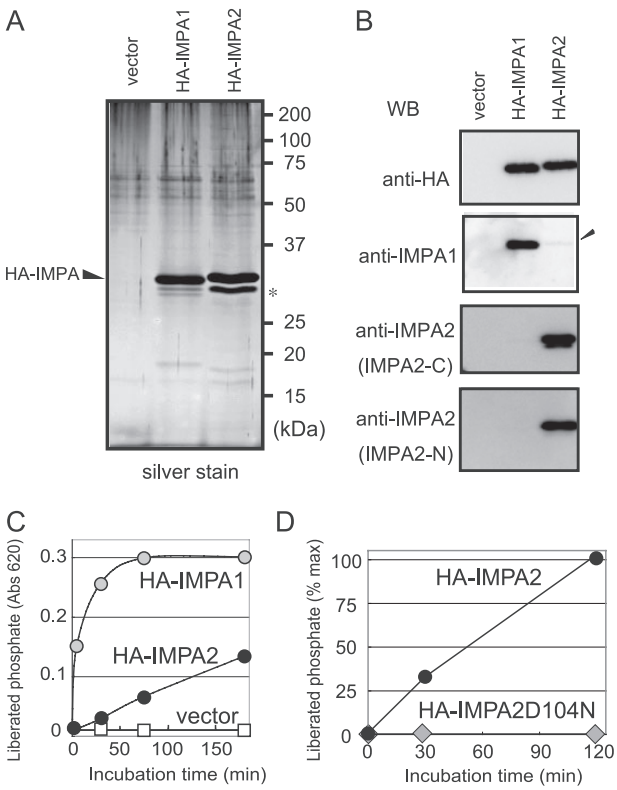

FIGURE 4. **Intrinsic IMPase activity of recombinant IMPA2.** *A*, recombinant proteins were purified using HA-affinity beads from HEK293T cells transfected with empty vector (*vector*), plasmid expressing HA-IMPA1 or HA-IMPA2. These preparations were analyzed by silver staining following SDS-PAGE. *B*, each preparation was analyzed by Western blotting using anti-HA, -IMPA1, or -IMPA2 (IMPA2-N and IMPA2-C). *C*, enzymatic activities of three preparations that dephosphorylate *myo*-inositol 1-monophosphate were examined using a calorimetric assay to detect phosphate liberated from substrate. *D*, lack of IMPase activity in HA-IMPA2 D104N.

the membrane fraction, most likely because of incomplete disruption of cells in the fractionation step; we cannot say with certainty that the IMPA2 protein exists in both the cytoplasmic and membrane fractions.

IMPA2 Forms Homodimers but No Heterodimers with IMPA1—Biochemical and x-ray crystallographic studies on IMPA1 show that the protein forms homodimers (16, 26). Because IMPA2 displayed strong amino acid homology (54%) with IMPA1 (Fig. 2*B*), we predicted that IMPA2 would also form homodimers and/or heterodimers with IMPA1. To test this theory, we first performed a co-immunoprecipitation assay. HA- or V5-tagged IMPA1 and IMPA2 (Fig. 2*B*) were transiently expressed as various combinations in HEK293T cells. As shown in Fig. 3*A*, V5-IMPA1 co-immunoprecipitated with HA-IMPA1, implying homodimerization of the protein. Similarly, we detected HA-IMPA2·V5-IMPA2 complexes in this assay, suggesting homodimerization of IMPA2. We did not detect V5-IMPA1·HA-IMPA2 or HA-IMPA1·V5-IMPA2 complexes, excluding the formation of heterodimers.

Next, we performed gel filtration column chromatography on protein extracts from HEK293T cells that transiently expressed V5-IMPA2. Subsequent Western blot analysis revealed that V5-IMPA2 eluted at around 70 kDa as a single peak without a shoulder (Fig. 3*B*). Because the calculated molecular mass of V5-IMPA2 is ~33 kDa, all pools of IMPA2 are likely to exist as homodimers *in vivo*. Moreover, ultracentrifugation sedimentation and x-ray crystallographic analyses of IMPA2 supported the proposed formation of homodimers (41).

Intrinsic IMPase Activity of IMPA2—Given that IMPA2 exhibits high primary structural similarity to IMPA1, we expected IMPA2 to have intrinsic IMPase activity. To examine this possibility, we prepared near homogeneously purified HA-IMPA2 and HA-IMPA1 proteins from cDNA-transfected HEK293T cells (Fig. 4*A*). Silver staining detected a minor band of faster mobility below the major band in HA-IMPA2 preparations (Fig. 4*A*, *asterisk*). This minor band was found to be IMPA2 by mass spectrometry (data not shown) and Western blot analysis using an anti-IMPA2 antibody (IMPA2-C, Fig. 2*B*). The IMPA2-C antibody detected a minor band as well as the major signal in HA-IMPA2 preparations (Fig. 4*B*, *third panel* from the *top*). A faint band was detected in the HA-IMPA2 preparation by the anti-IMPA1 antibody (Fig. 4*B*, *arrowhead*, *second panel* from the *top*). This was not because of contamination of endogenous IMPA1 protein because the migratory position of this band (~33 kDa) did not correspond to that of endogenous IMPA1 (~30 kDa). Because the antigenic region of the IMPA1 antibody was partially similar to the corresponding region of IMPA2 (Fig. 2*B*), the faint band in the IMPA2 prepara-

tion might be derived from nonspecific binding of the anti-IMPA1 antibody to HA-IMPA2 protein, and thus our IMPA2 preparation was still deemed to be immunologically pure.

Calorimetric determination revealed that the HA-IMPA2 preparation showed a time-dependent P_i inorganic phosphate releasing activity toward *myo*-inositol 1-monophosphate (Fig. 4*C*). The efficiency, however, was much lower than that of HA-IMPA1. One possibility was that the detected IMPase activity was not intrinsic but because of contaminating endogenous IMPA1 and/or an unknown phosphatase(s). To exclude this, we prepared an HA-IMPA2 D104N construct, where the 104th aspartatic residue of IMPA2 was substituted with asparagine (Fig. 2*B*). This mutant showed no activity (Fig. 4*D*), proving the intrinsic IMPase activity of IMPA2. Similarly, as the HA-IMPA1 D93N construct lost all activity (data not shown), the observed activity of HA-IMPA1 should also be innate.

Tissue purified IMPase is dependent on Mg^{2+} for activity (24, 26–28). We examined whether Mg^{2+} could be substituted by other metallic ions and found that both IMPA1 and IMPA2 elicited considerably weaker or almost no activity when Mg^{2+} was replaced by Ca^{2+}, Mn^{2+}, Na^+, or K^+ (2 mM each) (Fig. 5*A*). Therefore, we used magnesium chloride in subsequent assays. Interestingly, HA-IMPA2 had a different magnesium requirement compared with IMPA1 (Fig. 5*B*). HA-IMPA1 activity reached a maximum at sub-millimolar ranges of Mg^{2+}, then gradually declined at higher concentrations, as reported by other studies (24, 28). In contrast, HA-IMPA2 required a higher Mg^{2+} concentration (≥1 mM) for maximum activity and maintained this activity at all ranges of Mg^{2+} examined (Fig. 5*B*).

Attwood *et al.* (26) used a buffer containing 50 mM Tris-HCl (pH 8.0), 0.1 mM EGTA, and 2 mM $MgCl_2$ for assaying IMPase purified from bovine brain. We used this buffer but varied the pH to examine the pH dependence of IMPA1 and IMPA2 activity. We found that IMPA2 preferred a higher pH compared with IMPA1 (Fig. 5*C*). HA-IMPA1 showed maximum activity between pH 7.0 and 7.5, dropping to ~30% activity at pH 8.0. The activity of HA-IMPA2 was highest between pH 7.5 and 8.0. Thus, in a conventional assay containing 50 mM Tris-HCl at pH 8.0 and 2 mM $MgCl_2$, the activity of HA-IMPA1 is greatly underestimated, whereas that of HA-IMPA2 is near maximal.

Substrate Specificity—HA-IMPA1 efficiently dephosphorylated *myo*-inositol 1-monophosphate in our assay system, whereas HA-IMPA2 showed weak dephosphorylation activity. We estimated the relative activities of HA-IMPA1 and HA-IMPA2 toward *myo*-inositol 1-monophosphate as 6.9 and 0.50-nmol P_i release/μg protein/min, respectively (Fig. 5*E*). In addition, the reported K_m value of IMPA1 for *myo*-inositol 1-monophosphate was in the sub-millimolar range, whereas that of our HA-IMPA2 preparation was estimated at more than 5 mM (data not shown). This observation led to the theory that IMPA2 has a substrate specificity distinct from that of IMPA1 *in vivo*. The possible candidates included *myo*-inositol monophosphate phosphorylated at different positions, 2 through 6 (Fig. 5*D*). Accordingly, we synthesized these compounds and found on testing that they were only weakly dephosphorylated by HA-IMPA2 (Fig. 5*E*).

We continued to compare the substrate specificity of IMPA1 and IMPA2 in a standard assay by testing other compounds.

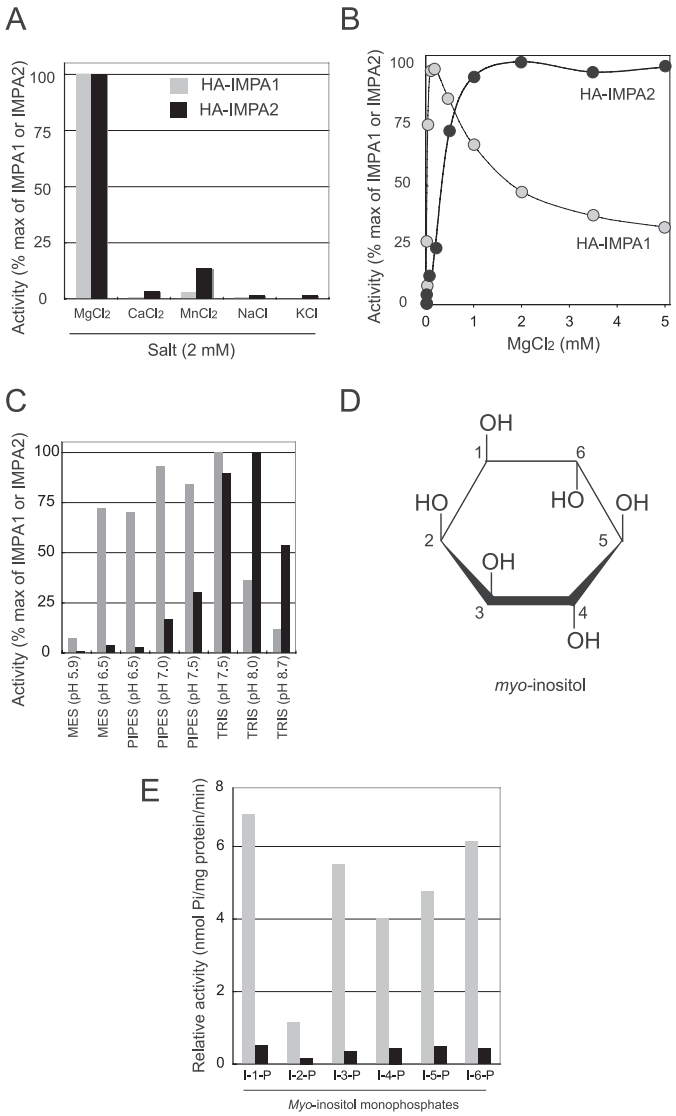

FIGURE 5. **Enzymatic profiles of IMPA2.** *A*, effects of various salts on IMPase activity. Data are shown as a percentage of the activity of HA-IMPA1 or -IMPA2 with salt relative to 2 mM $MgCl_2$. *B*, effects of varying concentrations of $MgCl_2$ on IMPase activities. Data are shown as a percentage of the maximum activity of HA-IMPA1 (*gray bar*) or -IMPA2 (*black bar*). *C*, effects of pH on IMPase activities. Buffering agents were MES, PIPES, or Tris. Data are shown as a percentage of the maximum activity of HA-IMPA1 or -IMPA2. *D*, structure of *myo*-inositol. Six carbon atoms of *myo*-inositol are denoted using the D numbering system. Note that the direction of the hydroxyl group at position 2 is reversed in *scyllo*-inositol. *E*, substrate specificity of IMPase activities. Six *myo*-inositol monophosphates (*I-1-P* through *I-6-P*) were tested. Data are shown as relative activity (*nmol P_i/mg protein/min*). *Gray* and *black bars* represent HA-IMPA1 and -IMPA2, respectively.

Based on the observation that *scyllo*-inositol is the second most abundant of the isomers of inositol (29, 30), we synthesized all possible *scyllo*-inositol phosphates and tested whether these compounds served as substrates for HA-IMPA2. Only *scyllo*-inositol 1,4-diphosphate was weakly dephosphorylated, other *scyllo*-inositols remained unchanged (Table 1). We extended this assay to other compounds, and these data are summarized in Table 1. We identified *myo*-inositol 1,4-diphosphate, glucose 1-phosphate, β-glycerophosphate, and 2′-AMP (2′-adenosine monophosphate) as *in vitro* substrates for IMPA2. However, the dephosphorylation efficiency of these compounds by HA-IMPA2 was very low compared with the efficiency with which

TABLE 1

Comparison of substrate specificity between IMPA1 and IMPA2

Relative catalytic activities are arbitrarily scaled between 1 and 10. ND, liberated phosphate not detected; −/+, trace amounts of released phosphate.

Compounds	IMPA1	IMPA2
***myo*-inositol-P_1**		
myo-inositol-1-P_1	10	2
myo-inositol-2-P_1	2	1
myo-inositol-3-P_1	10	2
myo-inositol-4-P_1	10	2
myo-inositol-5-P_1	10	2
myo-inositol-6-P_1	10	2
***myo*-inositol-P_2**		
myo-inositol-1,4-P_2	2	2
myo-inositol-1,5-P_2	−/+	ND
myo-inositol-3,4-P_2	ND	ND
myo-inositol-4,5-P_2	−/+	ND
***myo*-inositol-P_3**		
myo-inositol-1,2.3-P_3	ND	ND
myo-inositol-1,2.6-P_3	ND	ND
myo-inositol-1,3,4-P_3	ND	ND
myo-inositol-1,3,5-P_3	ND	ND
myo-inositol-1,3,6-P_3	ND	ND
myo-inositol-1,4,5-P_3	ND	ND
myo-inositol-1,4,6-P_3	ND	ND
myo-inositol-1,5,6-P_3	ND	ND
***myo*-inositol-P_4**		
myo-inositol-2,4,5-P_3	ND	ND
myo-inositol-3,4,5-P_3	ND	ND
myo-inositol-1,2,3,6-P_4	ND	ND
myo-inositol-1,2,5,6-P_4	ND	ND
myo-inositol-1,3,4,5-P_4	ND	ND
myo-inositol-1,3,5,6-P_4	ND	ND
myo-inositol-1,3,4,6-P_4	ND	ND
myo-inositol-1,4,5,6-P_4	ND	ND
myo-inositol-3,4,5,6-P_4	ND	ND
***myo*-inositol-P_5**		
myo-inositol-1,3,4,5,6-P_5	ND	ND
myo-inositol-1,2,3,4,5-P_5	ND	ND
***myo*-inositol-P_6**		
myo-inositol-P_6	ND	ND
***scyllo*-inositol-P**		
scyllo-inositol-P_1	8	−/+
L-*scyllo*-inositol-1,2-P_2	−/+	ND
D-*scyllo*-inositol-1,2-P_2	ND	−/+
scyllo-inositol-1,3-P_2	7	−/+
scyllo-inositol-1,4-P_2	4	2
scyllo-inositol-1,2,3-P_3	ND	ND
L-*scyllo*-inositol-1,2,4-P_3	ND	−/+
D-*scyllo*-inositol-1,2,4-P_3	ND	ND
scyllo-inositol-1,3,5-P_3	−/+	ND
L-*scyllo*-inositol-1,2,3,4-P_4	ND	ND
D-*scyllo*-inositol-1,2,3,4-P_4	ND	ND
scyllo-inositol-1,2,3,5-P_4	ND	ND
scyllo-inositol-1,2,4,5-P_4	ND	−/+
scyllo-inositol-P_5	ND	ND
scyllo-inositol-P_6	−/+	ND
Other sugar-phosphates		
Glucose-1-P_1	5	2
Glucose-6-P_1	2	ND
Fructose-1-P_1	2	ND
Fructose-6-P_1	−/+	ND
Fructose-1,6-P_2	−/+	ND
β-Glycerophosphate	7	2
2′-AMP	7	2
PIP		
PI-3-P_1	ND	ND
PI-4-P_2	ND	ND
PI-3,4-P_2	ND	ND

HA-IMPA1 dephosphorylated *myo*-inositol 1-monophosphate, indicating that the optimal substrate(s) for HA-IMPA2 are still to be determined.

Sensitivity to Lithium—Both recombinant IMPA1 and IMPase from mammalian tissues are inhibited by therapeutic concentrations of lithium (~1 mM) (10, 11, 24, 26, 27). Our

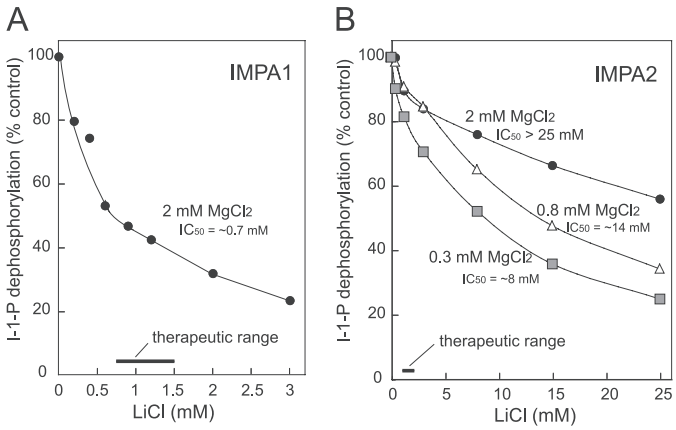

FIGURE 6. **Sensitivity of IMPA2 activity to lithium.** *A*, effects of varying concentrations (0–3 mM) of LiCl on the IMPase activity of IMPA1 at 2 mM $MgCl_2$. Data are shown as a percentage of activity in the absence of LiCl. *B*, effects of varying concentrations (0–25 mM) of LiCl and $MgCl_2$ (2, 0.8, or 0.3 mM) on the IMPase activity of IMPA2. Data from each $MgCl_2$ concentration are shown as a percentage of activity in the absence of LiCl.

HA-IMPA1 preparation also exhibited a similar sensitivity to lithium (IC_{50} = ~0.7 mM, Fig. 6*A*) in a conventional assay containing *myo*-inositol 1-monophosphate as a substrate and 2 mM $MgCl_2$. However, 1 mM lithium effected little change on the IMPase activity of HA-IMPA2 (Fig. 6*B*). Although the sensitivity to lithium was significantly increased at lower $MgCl_2$ concentrations (0.8 or 0.3 mM), decreased magnesium ions dampened the net IMPase activity of HA-IMPA2 (Fig. 5*B*). The IC_{50} values for lithium at 2, 0.8, and 0.3 mM $MgCl_2$ were approximately 25, 14, and 8 mM, respectively. At physiological concentrations of free Mg^{2+} (sub-millimolar range), the inhibition of IMPA2 at therapeutic concentrations (~1 mM) of lithium was ~10%.

Biological Consequences of IMPA1 or IMPA2 Knockdown—Finally, we assessed the biological effects of IMPA1- and/or IMPA2-siRNA treatment on the growth and morphology of HeLa Tet-Off cells. By siRNA transfection, we were able to attain >70% reduction of IMPA1 and IMPA2 proteins (Fig. 2*C* and data not shown) 2 days after transfection. The knockdown of either *IMPA1*, *IMPA2*, or both resulted in a similar growth rate (Fig. 7*A*) and morphology (Fig. 2*B*) to cells treated with control siRNA.

DISCUSSION

Until now, no study has confirmed the expression of IMPA2 protein *in vivo*. In this study, we demonstrated the endogenous expression of IMPA2 protein in a human tumor cell line Hela Tet-Off and various tissues from mice. We have also identified the following biochemical features of the *IMPA2* gene product (Fig. 8): 1) *IMPA2* transcripts are expressed in mouse brain with both overlapping and distinct patterns compared with *IMPA1*; 2) In the kidney and small intestine, *IMPA2* transcripts show a clear difference in tissue localization compared with *IMPA1*; 3) IMPA2 forms homodimers *in vivo* but no heterodimers with IMPA1; 4) IMPA2 has intrinsic IMPase activity that is completely dependent on magnesium, albeit this activity is much weaker than that of IMPA1 in our assay conditions; 5) IMPA2 has an optimal pH and magnesium concentration distinct to that of IMPA1; and 6) IMPase activity of IMPA2 is much less

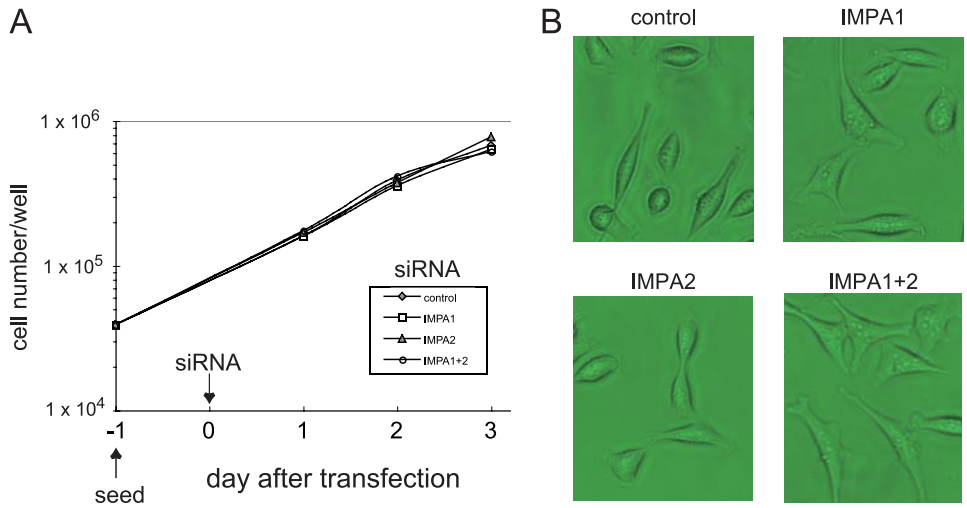

FIGURE 7. **Effects of IMPA1- or IMPA2-knockdown by siRNA on basic cell functions.** *A*, siRNA-treatment effect on the growth of HeLa Tet-Off cells. Twenty-four hours after seeding (day 1) on 6-well dishes, cells were transfected with siRNA (control siRNA, siRNA targeting *IMPA1* or *IMPA2*, or the mixture of siRNAs targeting *IMPA1* and *IMPA2*) (day 0). Cell numbers were counted at days 1, 2, and 3. *B*, cell morphology at day 2.

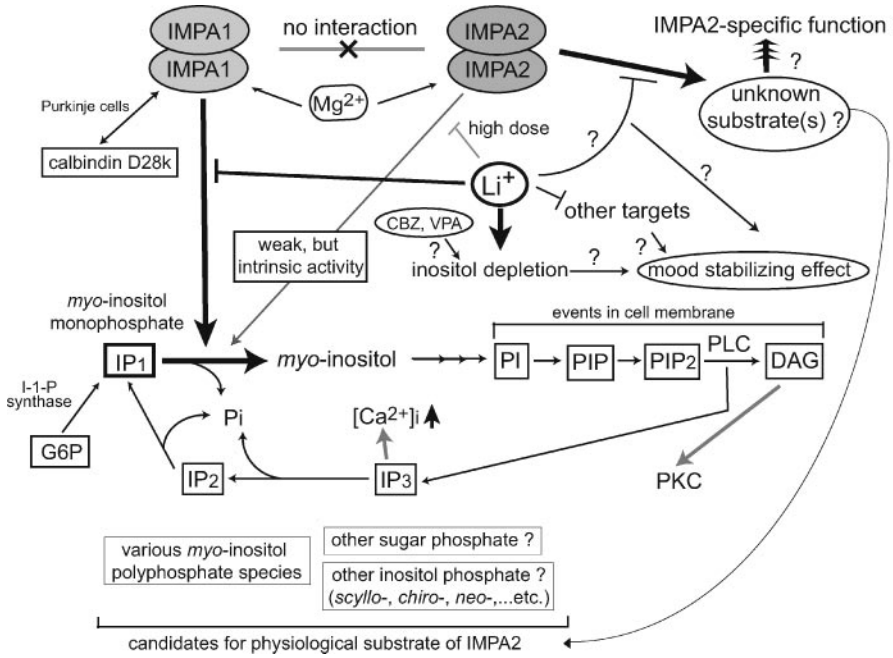

FIGURE 8. **Distinct functions of IMPA1 and IMPA2.** Data obtained from the present study are schematically summarized. See the text for details. *CBZ*, carbamazepine; *VPA*, valproic acid; IP_1, *myo*-inositol monophosphate; IP_2, *myo*-inositol bisphosphate; IP_3, *myo*-inositol 1,4,5-trisphosphate; *PLC*, phospholipase C; *PI*, phosphatidylinositol; *PIP*, phosphatidylinositol phosphate; PIP_2, phosphatidylinositol 4,5-bisphosphate; *G6P*, glucose 6-phosphate.

sensitive to lithium than that of IMPA1 when *myo*-inositol monophosphate is used as a substrate.

The x-ray crystallographic study of IMPA2 indicated that the protein had a slightly larger substrate pocket than that of IMPA1 (41). This may imply that the physiological substrate(s) for IMPA2 is a bulkier molecule than *myo*-inositol monophosphate. Many inositol phosphates with phosphoryl groups at different positions occur in cells, and their metabolic pathways are extremely complicated (31). Individual enzymes catalyzing the metabolism of inositol polyphosphates remain largely unknown. We tested inositol polyphosphates and *myo*-phosphatidyl inositol phosphates as potential larger molecules, but none of these served as optimal substrates for IMPA2 (Table 1). It is likely that IMPA2 has an as yet unidentified *in vivo* substrate(s). Recently, *myo*-inositol phosphate molecules with a pyrophosphate moiety have been proved to exist in cells (32–34). It would be of future interest to test whether these compounds serve as a good substrate for IMPA2. Alternatively, IMPA2 may require an undetermined activating co-factor(s) for full IMPase activity *in vivo*. Calbindin D28k, a calcium-binding protein enriched in the brain, has been reported as an activating binding partner for IMPA1 (35). A recent report showed that the interaction between calbindin D28k and IMPase, most likely IMPA1 (Fig. 8), arises in cerebellar Purkinje neurons and that interaction is required for the cellular localization of IMPase in spines and dendrites (36). Although *IMPA2* mRNA is expressed in Purkinje cells (Fig. 1) along with *IMPA1*, it is unlikely that calbindin D28k binds to IMPA2 because the amino acid sequence of the interaction site is poorly conserved in IMPA2. In HeLa Tet-Off cells and tissues of mice, IMPA2 is endogenously expressed as multiple bands in the range of ~32 kDa. It is tempting to think that IMPA2 activation requires intramolecular modifications such as phosphorylation and that the modified IMPA2 protein may correspond to the differently migrating band(s), although these issues are not addressed in this study.

Combining the evidence obtained in this study, we speculate that IMPA1 and IMPA2 may have separate biological functions targeting different physiological substrate(s). Although no apparent effects in the knockdown of *IMPA1* and *IMPA2* were observed (Fig. 7), we cannot rule out the possibility that these results were because of insufficient knockdown of the inositol monophosphatase proteins. Alternatively, biologically active *myo*-inositol may have been available from other pathways. For example, direct uptake from the extracellular milieu via *myo*-inositol transporters such as SMIT (Na^+-*myo*-inositol cotransporter) and HMIT (H^+-*myo*-inositol cotransporter). Conclusive proof on the specific biological role(s) of IMPA1 and IMPA2 requires further studies such as the analyses of mice deficient for each gene or cells separated from these mice.

Lithium is a mood stabilizer used to treat mood disorders.

However, lithium has a variety of side effects such as drowsiness, nausea, fatigue, polyuria, and hand tremors. In addition to its side effects, the therapeutic window of lithium is very narrow (0.6–1.5 mM in serum), making it essential to monitor the serum levels of the drug. To overcome these problems and develop new drugs with reduced unfavorable effects and improved efficacy, identification of the cellular targets of lithium is crucial. Several molecules are thought to be direct targets of lithium (1, 4). Among them, IMPase is one of the most cogent, leading to the inositol depletion hypothesis. In support of this hypothesis, recombinant IMPA1 (Fig. 6*A*) and IMPase purified from the brain are efficiently inhibited by lithium (26, 28, 37). However, concentrations of lithium in excess of the therapeutic range were needed to inhibit IMPase activity from IMPA2 in our assays when *myo*-inositol 1-monophosphate was used as a substrate. It is imperative to identify the intrinsic substrate(s) for IMPA2 and determine the lithium sensitivity of enzyme activity under physiological conditions. It is noteworthy that IMPA1 displays a substantial different sensitivity to lithium depending on the substrates used (26, 27).

Although there are overlapping tissue expression patterns of *IMPA1* and *IMPA2*, the epithelium of the intestinal glands in the small intestine and distal convoluted tubules of the kidney expressed only *IMPA2*. These facts suggest a specific role for IMPA2 that is not complemented by IMPA1 and may provide clues as to the biological distinctions between the two paralogous molecules. As stated earlier, one side of lithium is polyuria. This unfavorable effect may be related to the inhibition of IMPA1 and/or IMPA2 expression in the convoluted tubes of the kidney.

Numerous *in vitro* studies have used concentrations of lithium far in excess of the therapeutic dose (typically more than 10 mM) to examine its effects on cellular functions (38–40). Our data may imply that at least some of those reported effects are mediated by the inhibition of IMPA2. Further analyses of the IMPA2 protein are warranted to understand IMPA2-related biochemical abnormalities and molecular mechanisms of neuropsychiatric illnesses, and these efforts will help to develop biomarkers and better therapies for relevant diseases.

Acknowledgments—We thank Dr. Y. Hirabayashi (RIKEN Brain Science Institute) for useful suggestions and critically reading the manuscript. Authors also thank members of the Research Resources Center, RIKEN Brain Science Institute for technical assistance.

REFERENCES

1. Harwood, A. J. (2005) *Mol. Psychiatry* **10,** 117–126
2. Atack, J. R. (1996) *Brain Res. Brain Res. Rev.* **22,** 183–190
3. Atack, J. R., Broughton, H. B., and Pollack, S. J. (1995) *Trends Neurosci.* **18,** 343–349
4. Quiroz, J. A., Gould, T. D., and Manji, H. K. (2004) *Mol. Interv.* **4,** 259–272
5. Gould, T. D., and Manji, H. K. (2005) *Neuropsychopharmacology* **30,** 1223–1237
6. Zorrilla Zubilete, M. (2003) *Vertex* **14,** 45–52
7. Berridge, M. J., Downes, C. P., and Hanley, M. R. (1989) *Cell* **59,** 411–419
8. Berridge, M. J., and Irvine, R. F. (1989) *Nature* **341,** 197–205
9. Williams, R. S., Cheng, L., Mudge, A. W., and Harwood, A. J. (2002) *Nature* **417,** 292–295
10. Diehl, R. E., Whiting, P., Potter, J., Gee, N., Ragan, C. I., Linemeyer, D., Schoepfer, R., Bennett, C., and Dixon, R. A. (1990) *J. Biol. Chem.* **265,** 5946–5949
11. McAllister, G., Whiting, P., Hammond, E. A., Knowles, M. R., Atack, J. R., Bailey, F. J., Maigetter, R., and Ragan, C. I. (1992) *Biochem. J.* **284,** 749–754
12. Yoshikawa, T., Kikuchi, M., Saito, K., Watanabe, A., Yamada, K., Shibuya, H., Nankai, M., Kurumaji, A., Hattori, E., Ishiguro, H., Shimizu, H., Okubo, Y., Toru, M., and Detera-Wadleigh, S. D. (2001) *Mol. Psychiatry* **6,** 202–210
13. Nakayama, J., Yamamoto, N., Hamano, K., Iwasaki, N., Ohta, M., Nakahara, S., Matsui, A., Noguchi, E., and Arinami, T. (2004) *Neurology* **63,** 1803–1807
14. Sjoholt, G., Ebstein, R. P., Lie, R. T., Berle, J. O., Mallet, J., Deleuze, J. F., Levinson, D. F., Laurent, C., Mujahed, M., Bannoura, I., Murad, I., Molven, A., and Steen, V. M. (2004) *Mol. Psychiatry* **9,** 621–629
15. Yoshikawa, T., Turner, G., Esterling, L. E., Sanders, A. R., and Detera-Wadleigh, S. D. (1997) *Mol. Psychiatry* **2,** 393–397
16. Bone, R., Springer, J. P., and Atack, J. R. (1992) *Proc. Natl. Acad. Sci. U. S. A.* **89,** 10031–10035
17. Sadakata, T., Mizoguchi, A., Sato, Y., Katoh-Semba, R., Fukuda, M., Mikoshiba, K., and Furuichi, T. (2004) *J. Neurosci.* **24,** 43–52
18. Yamashita, A., Ohnishi, T., Kashima, I., Taya, Y., and Ohno, S. (2001) *Genes Dev.* **15,** 2215–2228
19. Ohnishi, T., Yamashita, A., Kashima, I., Schell, T., Anders, K. R., Grimson, A., Hachiya, T., Hentze, M. W., Anderson, P., and Ohno, S. (2003) *Mol. Cell* **12,** 1187–1200
20. Chung, S. K., Kwon, Y. U., Chang, Y. T., Sohn, K. H., Shin, J. H., Park, K. H., Hong, B. J., and Chung, I. H. (1999) *Bioorg. Med. Chem.* **7,** 2577–2589
21. Chung, S. K., and Chang, Y. T. (1996) *Korean J. Med. Chem.* **6,** 162–165
22. Seo, K. C., Yu, S. H., and Chung, S. K. (2006) *J. Carbohydr. Chem.*, in press
23. Yoshikawa, T., Padigaru, M., Karkera, J. D., Sharma, M., Berrettini, W. H., Esterling, L. E., and Detera-Wadleigh, S. D. (2000) *Mol. Psychiatry* **5,** 165–171
24. Takimoto, K., Okada, M., Matsuda, Y., and Nakagawa, H. (1985) *J. Biochem.* (*Tokyo*) **98,** 363–370
25. Meek, J. L., Rice, T. J., and Anton, E. (1988) *Biochem. Biophys. Res. Commun.* **156,** 143–148
26. Attwood, P. V., Ducep, J. B., and Chanal, M. C. (1988) *Biochem. J.* **253,** 387–394
27. Gee, N. S., Ragan, C. I., Watling, K. J., Aspley, S., Jackson, R. G., Reid, G. G., Gani, D., and Shute, J. K. (1988) *Biochem. J.* **249,** 883–889
28. Hallcher, L. M., and Sherman, W. R. (1980) *J. Biol. Chem.* **255,** 10896–10901
29. Fisher, S. K., Novak, J. E., and Agranoff, B. W. (2002) *J. Neurochem.* **82,** 736–754
30. Agranoff, B. W., and Fisher, S. K. (2001) *Psychopharmacol. Bull.* **35,** 5–18
31. Irvine, R. F., and Schell, M. J. (2001) *Nat. Rev. Mol. Cell Biol.* **2,** 327–338
32. Saiardi, A., Nagata, E., Luo, H. R., Sawa, A., Luo, X., Snowman, A. M., and Snyder, S. H. (2001) *Proc. Natl. Acad. Sci. U. S. A.* **98,** 2306–2311
33. Saiardi, A., Bhandari, R., Resnick, A. C., Snowman, A. M., and Snyder, S. H. (2004) *Science* **306,** 2101–2105
34. Nagata, E., Luo, H. R., Saiardi, A., Bae, B. I., Suzuki, N., and Snyder, S. H. (2005) *J. Biol. Chem.* **280,** 1634–1640
35. Berggard, T., Szczepankiewicz, O., Thulin, E., and Linse, S. (2002) *J. Biol. Chem.* **277,** 41954–41959
36. Schmidt, H., Schwaller, B., and Eilers, J. (2005) *Proc. Natl. Acad. Sci. U. S. A.* **102,** 5850–5855
37. Kennedy, S. P., Sha'afi, R. I., and Becker, E. L. (1988) *Biochem. Biophys. Res. Commun.* **155,** 189–196
38. Zhou, B. P., Deng, J., Xia, W., Xu, J., Li, Y. M., Gunduz, M., and Hung, M. C. (2004) *Nat. Cell Biol.* **6,** 931–940
39. Sarkar, S., Floto, R. A., Berger, Z., Imarisio, S., Cordenier, A., Pasco, M., Cook, L. J., and Rubinsztein, D. C. (2005) *J. Cell Biol.* **170,** 1101–1111
40. Stolovich, M., Lerer, T., Bolkier, Y., Cohen, H., and Meyuhas, O. (2005) *J. Biol. Chem.* **280,** 5336–5342
41. Arai, R., Ito, K., Ohnishi, T., Ohba, H., Akasaka, R., Bessho, Y., Hanawa-Suetsugu, K., Yoshikawa, T., Shirouzu, M., and Yokoyama, S. (2007) *Proteins Struct. Funct. Bioinformat.*, in press